Title

FATIGUE CRACK PROPAGATION IN DUAL-PHASE STEELS: EFFECTS OF FERRITIC-MARTENSITIC MICROSTRUCTURES ON CRACK PATH MORPHOLOGY

Authors

Dutta, V.B.
Suresh, S.
Ritchie, R.O.

Publication Date

1983-09-01

Lawrence Berkeley Laboratory
UNIVERSITY OF CALIFORNIA

Materials & Molecular Research Division

Submitted to Metallurgical Transactions A

FATIGUE CRACK PROPAGATION IN DUAL-PHASE STEELS: EFFECTS OF FERRITIC-MARTENSITIC MICROSTRUCTURES ON CRACK PATH MORPHOLOGY

V.B. Dutta, S. Suresh, and R.O. Ritchie

September 1983

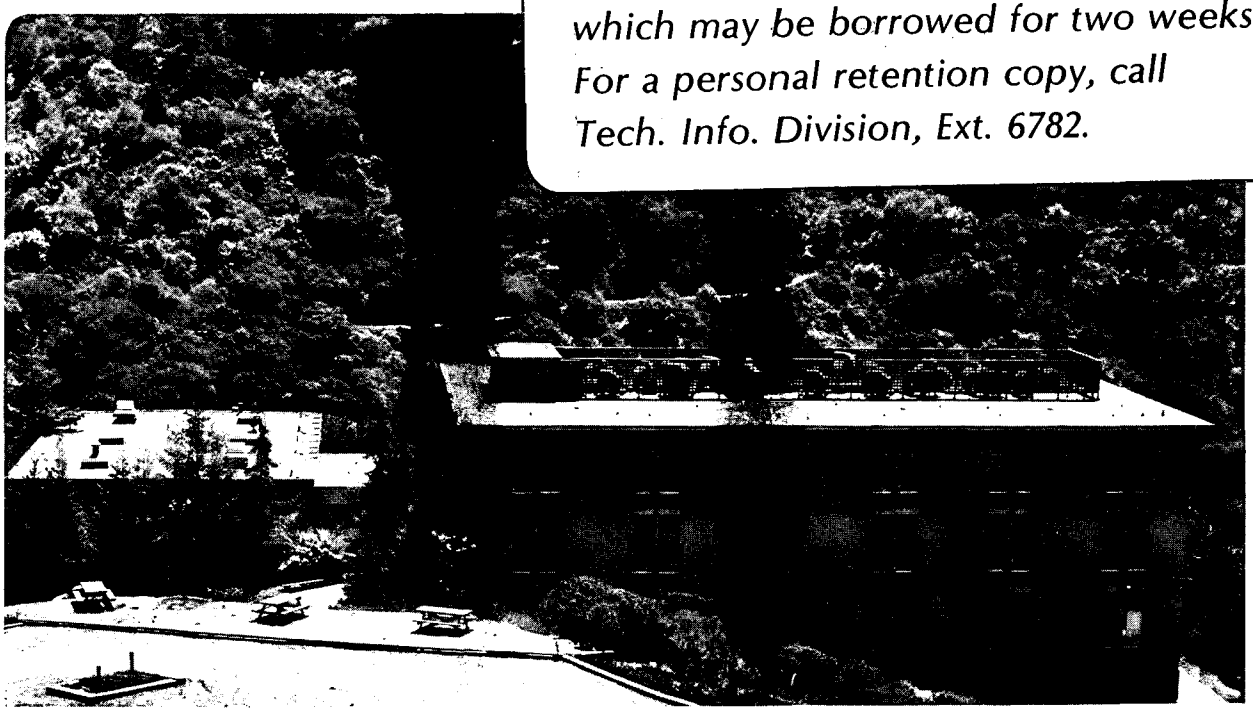

Prepared for the U.S. Department of Energy under Contract DE-AC03-76SF00098

DISCLAIMER

LBL-16264

FATIGUE CRACK PROPAGATION IN DUAL-PHASE STEELS: EFFECTS OF FERRITIC-MARTENSITIC MICROSTRUCTURES ON CRACK PATH MORPHOLOGY

V. B. Dutta,[1] S. Suresh[2] and R. O. Ritchie[1]

[1]Materials and Molecular Research Division, Lawrence Berkeley Laboratory, and Department of Materials Science and Mineral Engineering, University of California, Berkeley, CA 94720.

[2]Division of Engineering, Brown University, Providence, RI 02912. Formerly with the University of California, Berkeley, CA 94720.

September 1983

This work was supported by the Director, Office of Energy Research, Office of Basic Energy Sciences, Materials Sciences Division of the U.S. Department of Energy under Contract No. DE-AC03-76SF00098.

LBL-16264

FATIGUE CRACK PROPAGATION IN DUAL-PHASE STEELS: EFFECTS OF FERRITIC-MARTENSITIC MICROSTRUCTURES ON CRACK PATH MORPHOLOGY

V. B. Dutta, S. Suresh and R. O. Ritchie

ABSTRACT

Characteristics of fatigue crack propagation in dual-phase steels have been investigated in a high purity Fe-2Si-0.1C steel with the objective of developing ferritic-martensitic microstructures with maximum resistance to fatigue crack extension whilst maintaining high strength levels. A wide range of crack growth rates has been examined, from $\sim 10^{-8}$ to 10^{-3} mm/cycle, in a series of duplex microstructures of comparable yield strength and prior austenite grain size where inter-critical heat-treatments were used to vary the proportion, morphology and distribution of the ferrite and martensite phases. Results of fatigue crack propagation tests, conducted on "long cracks" in room temperature moist air environments, revealed a very large influence of microstructure over the entire spectrum of growth rates at low load ratios. Similar trends were observed at high load ratio, although the extent of the microstructural effects on crack growth behavior was

---

V. B. DUTTA is Graduate Student Research Assistant, Materials and Molecular Research Division, Lawrence Berkeley Laboratory, and Department of Materials Science and Mineral Engineering, University of California, Berkeley, CA 94720. S. SURESH, formerly Research Engineer in the Department of Materials Science and Mineral Engineering, University of California, Berkeley, CA 94720, is now Assistant Professor, Division of Engineering, Brown University, Providence, RI 02912. R. O. RITCHIE is Professor, Materials and Molecular Research Division, Lawrence Berkeley Laboratory, and Department of Materials Science and Mineral Engineering, University of California, Berkeley, CA 94720.

significantly less marked. Specifically, microstructures containing fine globular or coarse martensite in a coarse-grained ferritic matrix demonstrated exceptionally high resistance to crack growth without loss in strength properties. To our knowledge, these microstructures yielded the highest ambient temperature fatigue threshold stress intensity range ΔK_o values reported to date, and certainly the highest combination of strength and ΔK_o for steels (i.e., ΔK_o values above 19 MPa$\sqrt{m}$ with yield strengths in excess of 600 MPa). Such unusually high crack growth resistance is attributed primarily to a tortuous morphology of crack path which results in a reduction in the crack driving force from crack deflection and roughness-induced crack closure mechanisms. Quantitative metallography and experimental crack closure measurements, applied to simple analytical models for the deflection and closure processes, are presented to substantiate such interpretations.

1. INTRODUCTION

The role of microstructure in influencing the fatigue crack growth behavior in steels has been a subject of considerable research interest for many years. Recent studies (1-7) on lower growth rate behavior in ferritic, pearlitic, bainitic and martensitic steels have indicated that maximum resistance to fatigue crack extension can generally be achieved with coarse-grained microstructures of low cyclic yield strength, although the beneficial influence of grain size and strength level is seldom retained at high load ratios. Such microstructural effects on cyclic crack advance are found to be most significant in the near-threshold regime, below typically $\sim 10^{-6}$ mm/cycle, where stress intensity levels approach the threshold stress intensity range, ΔK_o, for no detectable growth of long cracks* (see refs. 1-5).

A particularly promising class of steels, where superior near-threshold fatigue resistance has been obtained without compromising strength, is the low carbon dual-phase steel. In this system, inter-critical heat treatments in the two phase ($\alpha + \gamma$) region lead to duplex structures consisting of ferrite (α) as the ductile matrix with a strong and tough second phase of low carbon martensite (α'). Such duplex steels, particularly those containing dislocated martensitic microstructures, show highly desirable tensile properties, such as continuous yielding from a low yield strength, high initial strain hardening rates and an excellent combination of tensile strength with ductility (8-12).

*The term "long crack" here refers to macro-cracks which are large compared to the scale of microstructure and/or the scale of local plasticity. When crack sizes approach such dimensions, so-called "short crack effects" have been observed where initiation and growth can occur at stress intensity levels below ΔK_o (for review, see ref. 8).

In terms of fatigue properties, the most dramatic results on the fatigue crack growth resistance of dual-phase steels were shown by McEvily and co-workers (14,15) who developed two different duplex microstructures in an AISI 1018 steel; one where a continuous ferrite matrix encapsulated islands of martensite (termed FEM or Type A in McEvily and co-workers' terminology (14,15)), and the other where a continuous martensitic phase encapsulated islands of ferrite (termed MEF or Type B). The former FEM microstructure showed properties similar to conventionally normalized AISI 1018 steel with a yield strength of 293 MPa and a fatigue threshold (at $R = K_{min}/K_{max} = 0.05$) of $\Delta K_o \approx 8$ MPa$\sqrt{m}$. However, the latter MEF microstructure showed a significant increase in <u>both</u> yield strength to 452 MPa and threshold ΔK_o values to 14 MPa$\sqrt{m}$. Subsequent studies (15) in AISI 1018 and 2¼Cr-1Mo steels confirmed the superior strength and <u>long crack</u> fatigue threshold properties of MEF, compared to conventionally heat-treated, microstructures and suggested that a high degree of connectivity of the martensite* and a large volume fraction of ferrite were important factors in duplex structures for achieving high thresholds with high strength. Such microstructures were reported to promote enhanced crack closure effects due to a more tortuous crack path, i.e., roughness-induced crack closure (6,16-19), and the high threshold values were correspondingly attributed to such closure (15). Based on similar tests in higher carbon steels, Minakawa et al. (15) found that such closure, and the resulting effects on ΔK_o values, were far less pronounced with higher volume fractions of martensite.

---

*The connectivity of the martensite is defined as the ratio of the number of ferrite/martensite boundaries per unit length to the number of boundaries (i.e., ferrite/martensite and ferrite/ferrite) per unit length, expressed as a percentage.

More recently, Wasynczuk et al. (20) have reported that long crack fatigue threshold ΔK_o values (at R = 0.05) for duplex microstructures in intercritically heat-treated AISI 1018 steels were unaffected by changes in the distribution and volume fraction (35 to 48 pct) of martensite, whereas similar microstructures in a simple Fe/2Si/0.1C steel showed 60 pct higher thresholds. As is characteristic with duplex microstructures (14,15,20-24), crack extension was not confined to either one of the two phases. However, crack paths were distinctly more tortuous in the Fe/2Si/0.1C steel, suggesting that the superior near-threshold fatigue resistance was again a consequence of enhanced roughness-induced closure.

Despite the unusually good near-threshold fatigue crack growth resistance of certain dual-phase microstructures for tests on long cracks, such properties are often not maintained in conventional fatigue limit/endurance strength tests. Based on studies which identified the fatigue limit in such structures as the stress intensity at which micro-cracks, initiated in the softer ferrite phase, were arrested in the harder martensite phase (21), Kunio, Yamada and co-workers (22,23) found that duplex microstructures in AISI 1023, 1025 and low alloy steels had only a minimal influence on short crack thresholds. For example, by comparing MEF and FEM structures in rotating bending tests on mild steel at R = -1, these authors report that the MEF microstructures, which were shown to have $\sim$ 75 pct higher threshold ΔK_o values for long cracks (i.e., 14 MPa$\sqrt{m}$ versus 8 MPa$\sqrt{m}$) (14), yielded essentially identical threshold values (i.e., between 7.4 and 7.9 MPa$\sqrt{m}$) when measured on short cracks between 0.5 and 1 mm in length.

Although duplex ferritic-martensitic microstructures appear promising from the point of view of designing alloys with improved resistance to high cycle fatigue crack growth, the results to date are often difficult to compare. Besides variations in distribution, morphology and volume fraction of each of the α and α' phases, important variables such as prior austenite grain size and strength level have previously not always been controlled. Moreover, all comparisons between the various dual-phase microstructures to date have only been performed at low load ratios, and before crack closure can be confirmed as a major factor influencing behavior, results and comparisons are required at high load ratios where the role of closure is known to be far less significant.

The rationale for the present work was to achieve maximum resistance to fatigue crack extension by developing duplex microstructures in a simple, high purity dual-phase steel which would promote meandering crack paths. By performing a series of carefully controlled experiments at both high and low load ratios on three different well-characterized ferritic/martensitic microstructures, with both prior austenite grain size and yield strength maintained constant, the objective was to elucidate mechanisms of microstructurally-influenced fatigue crack growth, and, based on these mechanisms, provide guidelines for the alloy design of dual-phase steels with superior resistance to fatigue.

2. EXPERIMENTAL PROCEDURES

Material

The material chosen for this investigation was a high purity Fe/2Si/0.1C steel of composition shown in Table I. This alloy was

developed as a dual-phase steel by Thomas and co-workers (9,13) and has been shown to display extremely good mechanical properties (e.g., ref. 13). The steel was vacuum induction melted, fully killed with rare earth additions, and cast in 23 kg ingots, before being vacuum-arc-remelted and homogenized in argon for 16 h at 1100°C. The ingot was then hot-forged at 850 to 1050°C to 76 mm square bars and controlled-rolled from 950 to 790°C to 13 mm thick plate. Oversized blanks for fatigue and uniaxial tensile tests were machined from the plate in the L-T orientation.

Heat Treatments and Microstructures

All blanks were first homogenized at 1200°C for 20 h and air cooled. Dual-phase, ferrite plus martensite, microstructures were then obtained using three different heat treatment cycles, adapted from the work of Kim and Thomas (13) but modified to achieve higher martensite concentrations, a constant prior austenite grain size of $\sim$ 240 μm and a constant yield strength of approximately 600 MPa. As shown in Fig. 1, all samples were first austenitized for 1 h at 1150°C whereupon i) the intermediate quenched (IQ) structures were iced-brine quenched, reheated intercritically for 40 mins at 1020°C and then re-quenched, ii) the step quenched (SQ) structures were rapidly cooled to 910°C in the ($\alpha + \gamma$) phase region, held for 40 mins and then iced-brine quenched, and iii) the intercritical annealed (IA) structures were air cooled to room temperature then reheated intercritically at 1010°C for 40 mins and then quenched.

Fatigue Crack Propagation Testing

All specimens were finally machined following heat treatment by removing a surface layer of at least 3.2 mm from all faces and edges. Since the last step in all the heat treatments involved a severe iced-brine quench, this procedure of excess machining was employed to minimize problems from residual stresses induced by quenching,* which are known to influence near-threshold crack growth behavior (25). Fatigue crack propagation rates, as a function of the alternating stress intensity factor ($\Delta K = K_{max} - K_{min}$), were obtained on 6.5 mm thick compact tension C(T) specimens tested under load control in 98 kN MTS electro-servo-hydraulic testing machines operating at a cyclic frequency of 50 Hz (sine wave). Tests were conducted in room temperature moist air (22°C, 30 pct relative humidity) at load ratios of R = 0.05 and 0.75, with all tests repeated at least once. D.C. electrical potential techniques were used to monitor continuously crack lengths, with near-threshold growth rates being determined under manual load shedding conditions. Such procedures are discussed in detail elsewhere (1,3,5).

Crack Closure Measurements

Macroscopic crack closure measurements were made by means of a set of six strain gauges affixed to each specimen in pairs at three locations such that at each point one gauge records strain parallel and the other perpendicular to the loading axis. As shown schematically in Fig. 2, gauges were placed on the side and back faces of the specimen, and the elastic compliance curves of load versus relative strain $|\varepsilon|$

*It might be noted that all subsequent fatigue fracture surfaces in such specimens showed extremely straight crack fronts with minimal bowing, indicating that any such residual stress effects were insignificant.

for all gauges monitored as a function of ΔK. Mean closure load values, obtained by averaging the point at which the six load versus relative strain plots ceased to be linear (Fig. 2), were utilized to compute a stress intensity at closure K_{cl} for each nominal ΔK level. Based on such measurements, the effective (near tip) stress intensity range, resulting from such closure, was defined as $\Delta K_{eff} = K_{max} - K_{cl}$.

3. RESULTS

Metallography and Mechanical Properties

Optical microscopy of the duplex microstructures resulting from the intermediate quench (IQ), step quench (SQ) and intercritical anneal (IA) transformation paths is shown in Fig. 1. As described in detail by Kim and Thomas (13), in the IQ process, reheating in the $(\alpha + \gamma)$ region after quenching from austenite results in the nucleation of austenite predominately along lath boundaries of prior martensite, giving rise to a fine fibrous martensite (58 vol pct) within a ferrite matrix. In the SQ process, step quenching from austenite into the $(\alpha + \gamma)$ region causes ferrite to nucleate at prior austenite grain boundaries and grow into the austenite, resulting in a coarse martensite (32 vol pct) surrounded by a continuous ferrite matrix. In the IA process, controlled air cooling from 1150°C results in a fine distribution of hypo-eutectoid ferrite plus pearlite microstructure which, on annealing in the $(\alpha + \gamma)$ region, causes austenite to nucleate on carbide/ferrite interfaces giving rise to a finer globular martensite (44 vol pct) along ferrite grain boundaries. A comparison of the room temperature uniaxial tensile curves together with the mechanical properties and

quantitative metallography are shown in Fig. 3 and Table II, respectively. The three microstructures display a range of ferrite grain sizes from 9 to 103 μm, and martensite volume fractions from 44 to 58 pct (with connectivities of 64 to 84 pct), but all have identical yield strengths within 6 pct of 600 MPa.

Fatigue Crack Propagation Behavior

The variation of fatigue crack propagation rates (da/dN) with stress intensity range ΔK for the IQ, SQ and IA microstructures is shown in Fig. 4 for load ratios of R = 0.05 and 0.75. A large influence of load ratio is apparent with threshold ΔK_o values being approximately a factor of 2 to 4 times smaller at R = 0.75 than at R = 0.05. More importantly, there is a very significant effect of the morphology of the duplex microstructure on fatigue crack growth behavior at low load ratios. This effect becomes far less pronounced at high load ratios, yet noticeable differences still exist between the different microstructures. Specifically at R = 0.05, growth rates below $\sim 10^{-5}$ mm/cycle are up to an order of magnitude slower in the step-quenched (SQ) and intercritical annealed (IA) structures, compared to the intermediate quenched (IQ) conditions, with threshold ΔK_o values being 60 to 82 pct higher (Table III). Whereas the threshold ΔK_o value at R = 0.05 is 10.7 MPa$\sqrt{m}$ for the IQ structure, the SQ and IA structures show ΔK_o values as high as 17.1 and 19.5 MPa$\sqrt{m}$, respectively. At R = 0.75, however, the range of threshold ΔK_o values for the microstructures is approximately 5 to 6 MPa$\sqrt{m}$.

The superior crack propagation resistance of the SQ and IA microstructures, compared to the IQ microstructure, is also maintained at higher growth rates above $\sim 10^{-6}$ mm/cycle (R = 0.05). It is, however, noticeable in Fig. 4 that the IA structure, which leads to

slower crack growth rates than the SQ structure at near-threshold levels, shows progressively faster growth rates than the latter structure above $\sim 10^{-5}$ mm/cycle. Specifically, the slope of the crack growth curve between 10^{-6} and 10^{-3} mm/cycle, i.e., the exponent m in the Paris power law relationship $da/dN \propto (\Delta K)^m$, is significantly larger for the IA microstructure (Table III).

Crack Closure Results

Values of the stress intensity at closure, K_{cl}, were obtained as function of the nominal stress intensity range ΔK during every test using the elastic compliance curves from back-face and side-face strain gauges (see Fig. 2). The results for the IQ, SQ and IA microstructures at both R = 0.05 and 0.75 are shown in Fig. 5 in the form of the ratio of closure to maximum stress intensity, K_{cl}/K_{max}, as a function of ΔK. Whereas no closure is detectable at high load ratios, the magnitude of the closure effect rapidly increases at low load ratios as ΔK approaches the threshold. Such results, which show the degree of closure to be at a maximum close to ΔK_o, are consistent with several recent observations on the near-threshold crack closure effect (e.g., refs. 6,7,15,17, 26,27). It is also clear that, at a given ΔK, the extent of closure is far greater for the microstructures showing the highest thresholds at R = 0.05, i.e., closure is enhanced in the IA and SQ rather than in the IQ structures, with the K_{cl}/K_{max} ratios at ΔK_o being between 0.7 to 0.8 in each case (Fig. 5).

Fractography

Scanning electron fractography of fatigue crack extension in the three microstructures at near-threshold levels and at higher growth rates (approximately at 10^{-5} mm/cycle) are shown in Figs. 6 and 7, respectively, for R = 0.05. The predominant fracture mode for all surfaces is transgranular, with the "hill-and-valley" type appearance commonly observed in low strength steels at lower stress intensities (28). At near-threshold levels (Fig. 6), fatigue fracture surfaces are coarser in appearance for the SQ and IA conditions, particularly for the SQ microstructure where there are clear indications of shear facets (e.g., Fig. 6(d)). The morphology of fracture surfaces in the IQ microstructure tends to be more planar (Fig. 6(a)) whereas in the SQ microstructure the fracture surface appears to change orientation about every 100 μm, i.e., of the order of the ferrite particle size (Fig. 6(c)). This faceted appearance is less obvious in the IA structure but occurs over somewhat larger dimensions of the order of the prior austenite grain size (Fig. 6(e)).

At higher growth rates, fracture surfaces remain transgranular and are rougher in the IA and particularly the SQ conditions, yet their overall appearance is distinctly smoother than at near-threshold levels (Fig. 7). However, the IA structure shows specific evidence of brittle cracking (i.e., static modes (29)) during fatigue crack growth in this regime, involving transgranular cleavage cracks through favorably orientated ferrite grains. The proportion of such cleavage facets, shown in Fig. 7(e), increases with increasing stress intensity levels from approximately 10 pct at $\sim 10^{-5}$ mm/cycle to approximately 50 pct

at $\sim 10^{-3}$ mm/cycle, consistent (29) with the higher slope in the crack growth curve (i.e., Paris Law exponent m) for this microstructure (Fig. 4).

Metallographic sections were also taken perpendicular to the fracture a few mm below the specimen surface to indicate crack path profiles. These are shown in Figs. 8, 9 and 10 for the IQ, SQ and IA microstructures, respectively, in both unetched and etched conditions to delineate clearly both crack shape and the specific influence of microstructural features on its direction. Points marked with an asterisk in these figures represent approximate locations where premature retardation (prior to ΔK_o) was experienced during standard load shedding procedures used to monitor near-threshold growth rates. Invariably, such abrupt reductions in growth rates, at stress intensity ranges well above ΔK_o, could be traced to sharp deflections in crack path and were particularly noticeable in the SQ and IA microstructures at low load ratios (Figs. 9 and 10). Based on these crack profiles, it is apparent that, irrespective of the ΔK level or load ratio, the crack propagates transgranularly in both the ferrite and martensite phases with almost equal preference, for all three microstructures. However, the profiles at both near-threshold and higher growth rates show evidence of crack deflections, where the crack path meanders, often rather sharply, from the plane of maximum tensile stress. The degree of deflection, though, varies significantly between the three conditions and becomes much more pronounced at lower growth rates and at low load ratios. In the intermediate quenched (IQ) structure (Fig. 8), few deflections are seen and the crack path is comparatively planar, consistent with its fine scale microstructure (Fig. 1) and smooth fracture surfaces (Fig. 6(a)). The step quenched (SQ)

structure, however, shows the most tortuous crack path (Fig. 9) consistent with its much coarser microstructure (Fig. 1) and rough fracture surfaces (Fig. 6(b)). Significant crack deflections tend to occur in this microstructure, with increasing regularity as the threshold is approached. The preferred sites for deflection generally are the ferrite/ferrite and ferrite/martensite interfaces (Fig. 11). Similar deflections in crack path (Fig. 10) and rough fracture surfaces (Fig. 6(b)), are found in the intercritical annealed (IA) structure.

4. DISCUSSION

The experiments conducted in this study on intermediate quenched (IQ), step quenched (SQ) and intercritical annealed (IA) structures in Fe/2Si/0.1C dual-phase steel were designed such that comparisons between radically different morphologies of duplex ferritic/martensitic microstructures could be made at constant prior austenite grain size ($\sim$ 240 μm) and yield strength ($\sim$ 600 MPa). The major differences in these microstructures occur in the ferrite particle size, which varies from 9 μm in the IQ structures to 103 μm in the SQ structures, and in the distribution, morphology and connectivity of martensite (Fig. 1). Although cleavage cracking through ferrite grains (Fig. 7(e)) leads to accelerated growth rates at high ΔK levels in the IA microstructure (Fig. 4), this structure together with the SQ microstructure offer by far the best fatigue resistance. Crack growth rates below $\sim 10^{-5}$ mm/cycle (which dominate in defect-tolerant life predictions) clearly indicate that, at R = 0.05, the coarser SQ and IA microstructures show the lower growth rates and higher thresholds (Fig. 4), consistent with their higher closure levels (Fig. 5),

rougher fracture surfaces (Fig. 6) and the more tortuous and deflected crack profiles (Figs. 7-11). The finer-scale IQ structure with far less closure (Fig. 5) and relatively planar fracture (Fig. 6) shows growth rates faster by a factor of $\sim$ 10 and threshold ΔK_o values lower by a factor of $\sim$ 2. Although the beneficial fatigue properties of the SQ and IA structures become significantly less pronounced at R = 0.75 (Fig. 4) because of a negligible effect of closure at high load ratios (Fig. 5), there exists a small but definite difference in the growth rates of the microstructures even at R = 0.75, presumably due to the differences in their crack deflection characteristics.

This relationship between superior crack growth resistance, non-linear, meandering crack paths and high closure loads in duplex microstructures clearly implies a dominant role of roughness-induced closure (6,15-19) and crack deflection (30) mechanisms.

Crack Closure Effects

Roughness-induced crack closure appears to be the most critical closure process responsible for the differences in fatigue behavior among the three microstructures because contributions from other sources of closure such as those due to cyclic plasticity (31) or oxide debris (32-34) are likely to be similar for these structures, with identical composition and yield strength, tested in identical environments. Such roughness-induced closure (6,15-19) arises from premature contact of the fracture surface asperities due to shear displacements which are not fully reversible because of inelastic crack-tip deformation and surface oxidation effects. This closure process is more pronounced at ΔK levels with crystallographic or faceted, mixed-mode crack growth, such as in the

near-threshold regime where the maximum plastic zone size is typically less than a characteristic microstructural unit size and the extent of fracture surface roughness is comparable to the crack tip opening displacements (6).

Based on simple geometric modelling, the extent of roughness-induced closure can be estimated from the relationship (19):

$$\frac{K_{cl}}{K_{max}} \approx \sqrt{\frac{2\gamma x}{1 + 2\gamma x}} \quad , \tag{1}$$

where x is the ratio of Mode II to Mode I crack tip displacements and γ is a nondimensional fracture surface roughness factor defined as the ratio of height to width of the fracture surface asperities. Predictions of the extent of closure can be made from Eq. (1) by using the crack path profiles for the three microstructures shown in Figs. 8 through 11 to estimate γ. Ignoring contributions from other sources of closure and assuming that x is of the order of unity,* predictions of K_{cl}/K_{max} (Table IV) for the three microstructures appear to be consistent with the experimentally measured trends in closure shown in Fig. 5. Such results further imply that the principal source of closure in the duplex microstructures arises from the roughness mechanism.

Crack Deflection Effects

Although crack closure is responsible for the major portion of differences in fatigue behavior among the three duplex morphologies, it does not account fully for all the observed variations in propagation

*This is clearly a simplification since the contribution to crack opening from Mode II displacements might be expected to increase as ΔK_o is approached (35).

rates with changes in microstructure. In Fig. 12(a), the experimental growth rate data at R = 0.05 for the IQ and SQ structures,* taken from Fig. 4, has been corrected for closure using the K_{cl} data from Fig. 5 such that growth rates are plotted as a function of ΔK_{eff} (= K_{max} - K_{cl}). It is clear from this figure that appreciable differences persist between the two microstructures (i.e., 30 to 40 pct changes in threshold ΔK_o values) even after crack closure has been accounted for. It, therefore, becomes necessary to consider additional mechanisms, such as crack deflection (30), to fully rationalize differences in fatigue characteristics for the duplex microstructures.

The present results clearly show a close correlation between resistance to fatigue crack propagation and the degree of non-linearity in crack path (c.f., Fig. 4 with Figs. 8 through 10). Whereas the intermediate quenched microstructure shows a highly linear crack path over the entire range of growth rates studied (Fig. 8), the step quenched and intercritically annealed microstructures show considerable tortuosities in crack path. Such deflections in crack path, away from the nominal Mode I growth plane, occur in the latter structures at ferrite/ferrite and ferrite/martensite interfaces (Figs. 9-11). Aside from promoting roughness-induced closure, such meandering crack path morphologies can lead to reduced effective (Mode I) stress intensities at the crack tip from the process of crack deflection alone.

---

*For the purposes of comparison, only the IQ and SQ structures have been analyzed here, since unlike the IA structure, behavior is not complicated at higher growth rates by the occurrence of brittle cleavage cracking through the ferrite (Fig. 7(e)). Furthermore, at near-threshold levels, growth rate, closure and crack path morphology data were similar in the SQ and IA structures.

This additional effect of crack path morphology can be quantitatively rationalized by considering the simple two dimensional crack deflection models, recently presented by Suresh (30). Such models account for the changes in effective driving force for deflected cracks and predict variations in crack extension rates for various degrees of deflection from the nominal Mode I growth direction. They incorporate the fact that a deflected crack i) requires an apparently larger driving force than a linear crack to propagate at the same velocity and ii) shows an apparently slower rate of growth than a linear crack subjected to the same nominal driving force wherever differences in crack profiles are ignored. For example, consider the idealization of a deflected crack profile shown in Fig. 12(b), where θ denotes the angle of deflection, D the distance over which the tilted crack advances along the kink and S the distance over which linear (Mode I) crack growth occurs, with such segments repeated over the crack length. Using two dimensional linear elastic analyses for the various degrees of deflection of this model crack, it has been shown (30) that the nominal driving force ΔK_{NL} for each segment of the deflected crack equals:

$$\Delta K_{NL} \approx \left[\frac{D \cos^2(\theta/2) + S}{D + S}\right]^{-1} \Delta K_L \quad , \qquad (2)$$

where ΔK_L is the corresponding driving force for a linear crack of the same length in the Mode I direction. In addition, the apparent (measured) growth rate $(\frac{da}{dN})_{NL}$ for this idealized deflected crack will always be smaller than the actual growth rate $(\frac{da}{dN})_L$, if crack path deflections are not considered, i.e.,

$$\left(\frac{da}{dN}\right)_{NL} \approx \left(\frac{D\cos\theta + S}{D + S}\right)\left(\frac{da}{dN}\right)_{L} \quad . \tag{3}$$

Eqs. (2) and (3) can be applied to the present case of duplex microstructures to estimate the individual contribution of crack deflection effects to the differences in microstructurally-sensitive crack growth behavior. Using the closure-corrected growth rate results for the IQ and SQ microstructures, plotted as a function of ΔK_{eff}, in Fig. 12(a), the da/dN vs. ΔK_{eff} data for the IQ structure are taken as a reference line with $\theta = 0°$, since this microstructure shows markedly less pronounced deflections in crack path compared to the other structures (c.f., Figs. 8 to 10). If this relatively linear crack is now allowed to deflect, Eqs. (2) and (3) suggest the fatigue crack growth curve will be shifted to the right to a degree dependent upon θ and $\frac{D}{D + S}$, and the extent of this shift will be an indication of the contribution from crack deflection (30). Quantifying the large degree of deflection in the step quenched (SQ) microstructure is difficult since the extent of crack path meandering is not uniform and tends to be more pronounced at lower growth rates. However, choosing typical values of the angle of tilt θ of 45° to 75° with $\frac{D}{D + S}$ between 0.25 and 0.5 for the SQ structure, predictions of the improvements in fatigue crack growth characteristics compared to the IQ structure (where $\theta = 0°$), due only to changes in deflection behavior, are shown by the dashed lines in Fig. 12(b) for R = 0.05. Thus, the process of crack deflection in the step-quenched (SQ) microstructure alone can account for up to a 30 pct increase in threshold ΔK_o at R = 0.05, compared to the IQ microstructure, without incorporating closure effects. This is also apparent by considering high load ratio

behavior where closure effects are minimal. Similar predictions for $R = 0.75$, shown in Fig. 13, suggest that the small, but reproducible, differences in fatigue response between the three duplex microstructures can also be traced to crack deflection by again assuming reasonable values for θ and $\frac{D}{D + S}$.

Thus the major improvement in resistance to fatigue crack propagation observed in the SQ and IA microstructures, compared to the IQ structure, has been rationalized in terms of the coarser duplex morphologies promoting a more tortuous crack path, which in turn leads to a reduction in effective (near-tip) driving force due to crack deflection and principally roughness-induced closure effects. The relative contributions from these two mechanisms can be appreciated in Fig. 12 where the separate effects of closure and deflection have been plotted based on the experimental closure data in Fig. 5 and the deflection model predictions from Eqs. (2) and (3).

The prominant role of closure in inducing such microstructurally-sensitive crack advance in dual-phase steels is consistent with experimental observations of a much smaller effect of microstructure on near-threshold crack growth at high load ratios (Fig. 4) and at short crack lengths (22,23). Since this closure mechanism can only be effective where minimum crack tip opening displacements do not exceed the size-scale of the fracture surface roughness, its contribution at high load ratios must become insignificant (6,19), as verified by the experimental closure measurements in Fig. 5. Moreover, since any physical contact between crack faces occurs in the wake of the crack tip, and since by definition, short cracks possess only a limited wake, the contribution from such closure must also be lessened at small crack lengths (8,19,36). This

is presumably why the continuous martensitic MEF microstructures developed by McEvily et al. (14,15), which showed such high long crack threshold values at low load ratios, failed to reveal such enhanced fatigue properties and behaved no better than normalized structures when evaluated using fatigue limit and short crack threshold tests (23).

Static Mode Effects

Intrinsic metallurgical effects would appear to be of lesser importance for fatigue crack propagation resistance in dual-phase steels since only marginal differences in behavior are observed at high load ratios (Fig. 4). However, in addition to the closure and deflection processes, microstructurally-sensitive crack growth can result at higher stress intensity levels from the occurrence of brittle fracture modes. As noted previously by others (20,24), certain duplex microstructures are prone to suffer transgranular cleavage cracking through ferrite grains at higher growth rates, as indicated by the intercritical annealed (IA) structures in the present work (Fig. 7(e)). Although unimportant to behavior below typically $\sim 10^{-5}$ mm/cycle, such cleavage cracking during cyclic crack advance leads to faster growth rates and higher Paris power law exponent m values at high ΔK levels, and is a good example of the role of "static" or monotonic fracture modes in accelerating crack propagation rates, as commonly observed in lower toughness materials (29,37,38).

Thus, in summary, based on the present study for dual-phase Fe/2Si/0.1C steel, it would appear that duplex microstructures containing fine globular or coarse martensite within a coarse-grained ferrite matrix, such as shown by the step quenched (SQ) and intercritical annealed (IA) structures,

offer unusually high fatigue crack growth resistance, particularly at near-threshold levels, with no loss in strength. Although IA microstructures show a tendency for progressively accelerated growth rates above $\sim 10^{-5}$ mm/cycle due to cleavage cracking in the ferrite, the superior crack growth resistance of both SQ and IA microstructures can be traced to meandering crack path morphologies which result in a lowering of the effective (near-tip) driving force for crack advance principally due to roughness-induced crack closure and crack deflection mechanisms.

5. CONCLUDING REMARKS

It is clear from the present, and previous (14,15,20), studies on dual-phase steels that duplex ferritic/martensitic microstructures can have a remarkable influence on resistance to fatigue crack propagation of long cracks, without causing any loss in strength. Such superior fatigue resistance is apparent over the entire range of growth rates (i.e., $\sim 10^{-8}$ to 10^{-3} mm/cycle) but is particularly marked below $\sim 10^{-6}$ mm/cycle in the near-threshold regime where ΔK_o values at low load ratios can be dramatically increased. For the majority of steels such major increases in threshold values are only achieved by marked reductions in strength level (1,3,5). Yet as previously noted by Suzuki and McEvily (14), the remarkable aspect of dual-phase steels is that the higher long crack ΔK_o values measured in certain duplex microstructures are generally associated with increased strength level. This can be appreciated in Fig. 14 where low load ratio threshold ΔK_o values are plotted as a function of monotonic yield strength ($\sigma_y \approx 200$ to 1800 MPa) for a wide range of ferritic, pearlitic, bainitic and martensitic steels, taken from

reference sources in refs. 1 and 5. The data points for duplex ferritic/martensitic microstructures can be seen in many instances to lie well above the scatter band indicating the superior fatigue threshold and strength properties of these dual-phase steels. In particular, the data for Fe/2Si/0.1C from the present study, where step-quenched (SQ) and intercritical annealed (IA) microstructures were developed with yield strengths in excess of 600 MPa and long crack, low load ratio, threshold ΔK_o values as high as 17.1 and 19.5 MPa$\sqrt{m}$, respectively, may well represent the highest combinations of fatigue threshold and yield strength measured to date. Furthermore, based on these results in Fig. 14, the present SQ and IA duplex microstructures show a 43 to 64 pct increase in threshold ΔK_o compared to the previous highest threshold at this strength level. In fact the ΔK_o values measured at R = 0.05 for the intercritical annealed (IA) microstructures are to the authors' knowledge the highest ambient temperature fatigue threhsolds ever reported for ferrous alloys, and further represent over an 80 pct increase in ΔK_o over the intermediate quenched (IQ) structure <u>at the same strength level</u>.

In the present study we further confirm that such unusually high fatigue crack propagation resistance can be attributed to the formation of tortuous crack path morphologies in the duplex microstructures. Further, we quantitatively evaluate the consequent effect of such crack paths on the effective (near-tip) driving force for crack advance in terms of crack deflection and roughness-induced crack closure processes, using quantitative metallography, experimental closure measurements and simple modelling concepts. However, due to the predominance of crack closure mechanisms in causing the reduced growth rates in such

dual-phase microstructures, it must be noted that the superior fatigue resistance of such structures is unlikely to be maintained at high load ratios or in the presence of short cracks where closure effects are less relevant. This is apparent from the present results of a minimal effect of microstructure on fatigue thresholds and crack growth rates at R = 0.75 (Fig. 4) and by observations (22,23) that duplex microstructures, which show superior ΔK_0 values in long crack tests, are no better than conventionally normalized structures when compared on the basis of classical fatigue limits or thresholds for short crack growth.

6. CONCLUSIONS

Based on a study in an intercritically heat-treated high purity, dual-phase Fe/2Si/0.1C steel where duplex ferritic/martensitic microstructures, of varying morphologies yet similar strength levels ($\sigma_y \sim 600$ MPa), were developed with the objective of enhancing fatigue crack growth resistance, the following conclusions can be made:

1) The morphology of the duplex microstructure was found to have a profound influence on rates of fatigue crack growth at R = 0.05 over a wide range from $\sim 10^{-8}$ to 10^{-3} mm/cycle, without changes in strength level. Although behavior was essentially similar at high load ratios (i.e., R = 0.75), the effect was considerably reduced.

2) Coarse or fine globular martensitic structures within a coarse-grained ferritic matrix, obtained through step quenching (SQ) and intercritical annealing (IA), respectively, were found to have substantially improved fatigue resistance over very fine fibrous martensitic/ferritic structures produced by intermediate quenching (IQ), although the IA

microstructure was prone to cleavage cracking in the ferrite above $\sim 10^{-5}$ mm/cycle. Specifically, growth rates in the SQ structure were 10 to 20 times slower than in the IQ structure at R = 0.05, with threshold ΔK_o values in the SQ and IA structures increased from 11 MPa$\sqrt{m}$ to 17.1-19.5 MPa$\sqrt{m}$.

3) The markedly reduced growth rates in the SQ and IA structures were found to be consistent with high measured levels of crack closure, rough faceted fracture surfaces, and meandering crack path morphologies due to deflection at ferrite/ferrite and ferrite/martensite interfaces.

4) Using simple modelling concepts, the superior fatigue crack growth resistance of the SQ and IA structures was attributed to reduction in effective driving force at the crack tip due to enhanced crack deflection and principally to enhanced roughness-induced crack closure, reuslting from the meandering crack paths. Quantitative estimates suggest that the specific contributions from these deflection and closure mechanisms were in the ratio 1:2.

5) The present step quenched and intercritical annealed duplex microstructures show usually high "long crack" fatigue resistance at low load ratios. In fact, the observed ΔK_o values of 17.1 and 19.5 MPa$\sqrt{m}$, respectively, with a yield strength of 600 MPa, are believed to be the highest ambient temperature fatigue thresholds ever reported and certainly represent the highest combination of fatigue threshold and yield strength measured for steels to date.

Acknowledgements

The work was supported by the Director, Office of Energy Research, Office of Basic Energy Sciences, Materials Sciences Division of the U.S. Department of Energy, under Contract No. DE-AC03-76SF00098. The authors would like to thank Professor G. Thomas and Dr. N. J. Kim for helpful discussions and Professor Thomas for providing the Fe/2Si/0.1C steel.

References

1. R. O. Ritchie: Int. Metall. Rev., 1979, vol. 20, p. 205.
2. J. Masounave and J.-P. Baïlon: Scripta Met., 1976, vol. 10, p. 165.
3. R. O. Ritchie: Metal Science, 1977, vol. 11, p. 368.
4. J. P. Lucas and W. W. Gerberich: Mater. Sci. Eng., 1981, vol. 51, p. 203.
5. S. Suresh, G. F. Zamiski, and R. O. Ritchie: in Application of 2¼Cr-1Mo Steel for Thick Wall Pressure Vessels, ASTM STP 755, G. S. Sangdahl and M. Semchyshen, eds., American Society for Testing and Materials, Philadelphia, PA, 1982, pp. 49-67.
6. R. O. Ritchie and S. Suresh: Metall. Trans. A, 1982, vol. 13A, p. 937.
7. G. T. Gray, A. W. Thompson, and J. C. Williams: Metall. Trans. A, 1983, vol. 14A, p. 421.
8. S. Suresh and R. O. Ritchie: Int. Metall. Rev., 1983, vol. 24, in review (University of California, Berkeley, Report No. UCB/RP/83/A1014, June 1983).
9. J. Y. Koo and G. Thomas: Metall. Trans. A, 1977, vol. 8A, p. 525.
10. Y. Tomota, N. Tachibana, and K. Kuroki: Trans. ISIJ, 1978, vol. 18, p. 251.
11. G. R. Speich: in Fundamentals of Dual-Phase Steel, R. A. Kot and B. L. Bramfitt, eds., The Metallurgical Society of AIME, Warrendale, PA, 1981, p. 3.
12. R. G. Davies: Metall. Trans. A, 1978, vol. 9A, p. 41.
13. N. J. Kim and G. Thomas: Metall. Trans. A, 1981, vol. 12A, p. 483.
14. H. Suzuki and A. J. McEvily: Metall. Trans. A, 1979, vol. 10A, p. 475.

15. K. Minakawa, Y. Matsuo, and A. J. McEvily: Metall. Trans. A, 1982, vol. 13A, p. 439.

16. N. Walker and C. J. Beevers: Fat. Eng. Mat. Struct., 1979, vol. 1, p. 135.

17. K. Minakawa and A. J. McEvily: Scripta Met., 1981, vol. 15, p. 633.

18. I. C. Mayes and T. J. Baker: Fat. Eng. Mat. Struct., 1981, vol. 4, p. 79.

19. S. Suresh and R. O. Ritchie: Metall. Trans. A, 1982, vol. 13A, p. 1627.

20. J. A. Wasynczuk, R. O. Ritchie, and G. Thomas: Mater. Sci. Eng., 1983, in press.

21. T. Kunio and K. Yamada: in Fatigue Mechanisms, ASTM STP 675, J. T. Fong, ed., American Society for Testing and Materials, Philadelphia, PA, 1979, pp. 342-361.

22. T. Kunio, M. Shimizu, K. Yamada, and H. Nakabayashi: in Fatigue Thresholds, J. Bäcklund, A. Blom, and C. J. Beevers, eds., EMAS Ltd., Warley, U.K., 1982, vol. 1, pp. 409-422.

23. K. Yamada: Discussion in Fatigue Mechanisms, ASTM STP 675, J. T. Fong, ed., American Society for Testing and Materials, Philadelphia, PA, 1979, p. 367.

24. T. Ishihara: in Mechanical Behavior of Materials-IV, Proceedings of Fourth Intl. Conf. (ICM-4), Stockholm, Sweden, J. Carlsson and N. G. Ohlson, eds., Pergamon Press, New York, 1983, vol. 2, p. 1155.

25. R. J. Bucci: in Fracture Mechanics (13th Conference), ASTM STP 743, American Society for Testing and Materials, Philadelphia, PA, 1981, p. 28.

26. P. K. Liaw, T. R. Leax, R. S. Williams, and M. G. Peck: Metall. Trans. A, 1982, vol. 13A, p. 1607.

27. W. W. Gerberich, W. Yu, and K. Esaklul: Metall. Trans. A, 1983, vol. 14A, in review.

28. G. Birkbeck, A. E. Inckle, and G. W. J. Waldron: J. Mat. Sci., 1971, vol. 6, p. 319.

29. R. O. Ritchie and J. F. Knott: Acta Met., 1973, vol. 21, p. 639.

30. S. Suresh: Metall. Trans. A, 1983, vol. 14A, in press (University of California, Berkeley, Report No. UCB/RP/83/A1011, Feb. 1983).

31. W. Elber: Eng. Fract. Mech., 1970, vol. 2, p. 37.

32. R. O. Ritchie, S. Suresh, and C. M. Moss: J. Eng. Matls. Tech., Trans. ASME Series H, 1980, vol. 102, p. 293.

33. A. T. Stewart: Eng. Fract. Mech., 1980, vol. 13, p. 463.

34. S. Suresh, G. F. Zamiski, and R. O. Ritchie: Metall. Trans. A, 1981, vol. 12A, p. 1435.

35. D. L. Davidson: Fat. Eng. Mat. Struct., 1981, vol. 3, p. 229.

36. J. F. McCarver and R. O. Ritchie: Mater. Sci. Eng., 1982, vol. 55, p. 63.

37. C. E. Richards and T. C. Lindley: Eng. Fract. Mech., 1972, vol. 4, p. 951.

38. R. O. Ritchie and J. F. Knott: Mater. Sci. Eng., 1974, vol. 14, p. 7.

Table I. Composition in Wt. Pct. of Fe/2Si/0.1C Steel

C	Si	Mn	S	P	Cr	Ni	Mo	V
0.09	2.01	<0.005	<0.005	0.005	<0.005	0.06	0.03	<0.01

Table II. Quantitative Metallography and Uniaxial Tensile Properties for Fe/2Si/0.1C Dual-Phase Steel

Heat Treatment	Prior Austenite Grain Size (μm)	Ferrite Particle Size (μm)	Vol. Fract. Martensite (pct)	Connectivity of Martensite (pct)	Yield Strength (MPa)	UTS (MPa)	Redn. Area (pct)
IQ	237	9	58	84	590	805	71
SQ	237	103	32	64	635	900	33
IA	237	27	44	82	615	827	53

Table III. Fatigue Crack Propagation Results for Fe/2Si/0.1C Dual-Phase Steel

Heat Treatment	Threshold ΔK_o (MPa$\sqrt{m}$)		Maximum Extent of Closure K_{cl}/K_{max} at ΔK_o		Paris Law Exponent*
	R = 0.05	R = 0.75	R = 0.05	R = 0.75	m
IQ	10.7	4.9	0.74	0	4.8
SQ	17.1	5.1	0.83	0	5.3
IA	19.5	5.7	0.78	0	9.3

*Derived from crack growth data at R = 0.05 above 10^{-6} mm/cycle by regression fit to Paris relationship: $da/dN \propto (\Delta K)^m$.

Table IV. Predicted and Experimentally Measured Closure Values in Terms of K_{cl}/K_{max} as a Function of ΔK

Heat Treatment	ΔK ($MPa\sqrt{m}$)	γ	Predicted K_{cl}/K_{max} (from Eq. 1)	Measured K_{cl}/K_{max} (from Fig. 5)
IQ	14.8	0.20	0.53	0.45
IQ	10.7	0.30	0.61	0.74
SQ	25.9	0.40	0.66	0.51
SQ	22.8	0.45	0.68	0.58
SQ	17.1	0.40	0.66	0.80
IA	19.5	0.45	0.68	0.75

NOMENCLATURE

a	crack length
D	length of deflected segment of crack
da/dN	fatigue crack growth rate per cycle
$(da/dN)_L$	average growth rate of linear crack
$(da/dN)_{NL}$	average growth rate of non-linear crack
IA	intercritical anneal
IQ	intermediate quench
K	Mode I stress intensity factor
K_{cl}	stress intensity factor at closure of crack
K_{max}, K_{min}	maximum and minimum stress intensity factors, respectively
ΔK	alternating stress intensity factor ($K_{max} - K_{min}$)
ΔK_L	average stress intensity range for linear crack
ΔK_{NL}	average stress intensity range for non-linear crack
ΔK_{eff}	effective stress intensity range ($K_{max} - K_{cl}$)
ΔK_o	threshold stress intensity range for no growth of long crack
m	exponent in Paris Law: $da/dN \propto \Delta K^m$
N	number of cycles
P_{max}, P_{min}	maximum and minimum load, respectively, during cycle
P_{cl}	load at closure of crack
R	load (or stress) ratio (K_{min}/K_{max})
S	length of linear segment of crack
SQ	step quench
UTS	ultimate tensile strength
x	ratio of Mode II to Mode I crack tip displacements (u_{II}/u_I)
γ	non-dimensional fracture surface roughness factor
$\|\varepsilon\|$	relative strain
θ	angle of deflection of crack
σ_y	yield strength

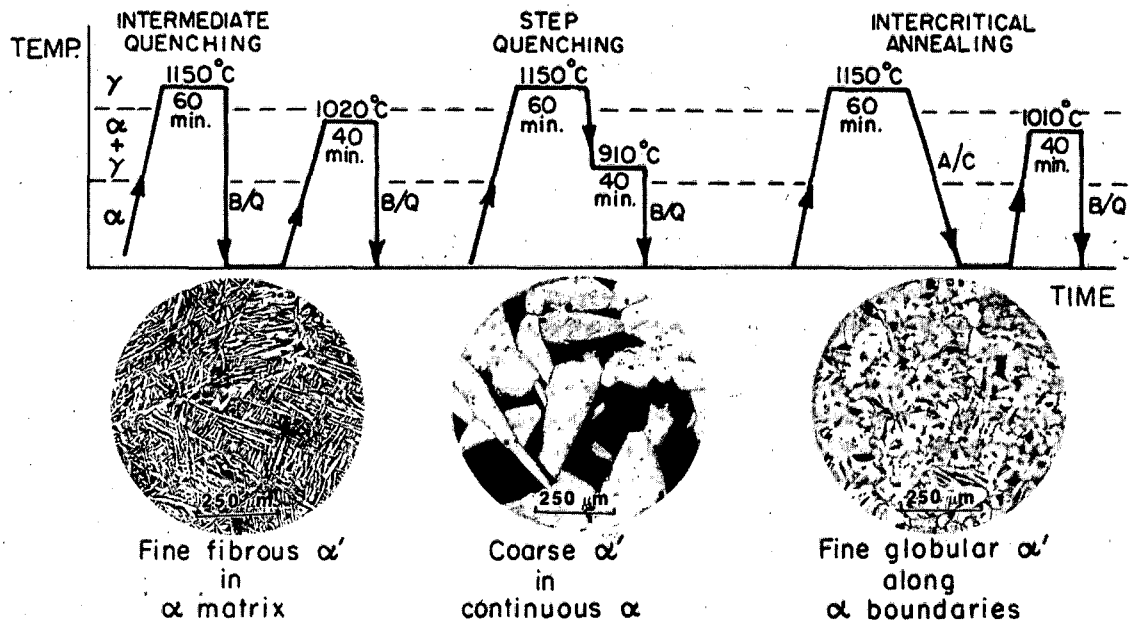

XBB 833-2300

Fig. 1: a) Heat-treatment cycles and b) resulting duplex microstructures in Fe/2Si/0.1C dual-phase steel following intermediate quenching (IQ); step quenching (SQ) and intercritical annealing (IA) (etched in 5 pct nital). All microstructures have a constant yield strength of approximately 600 MPa.

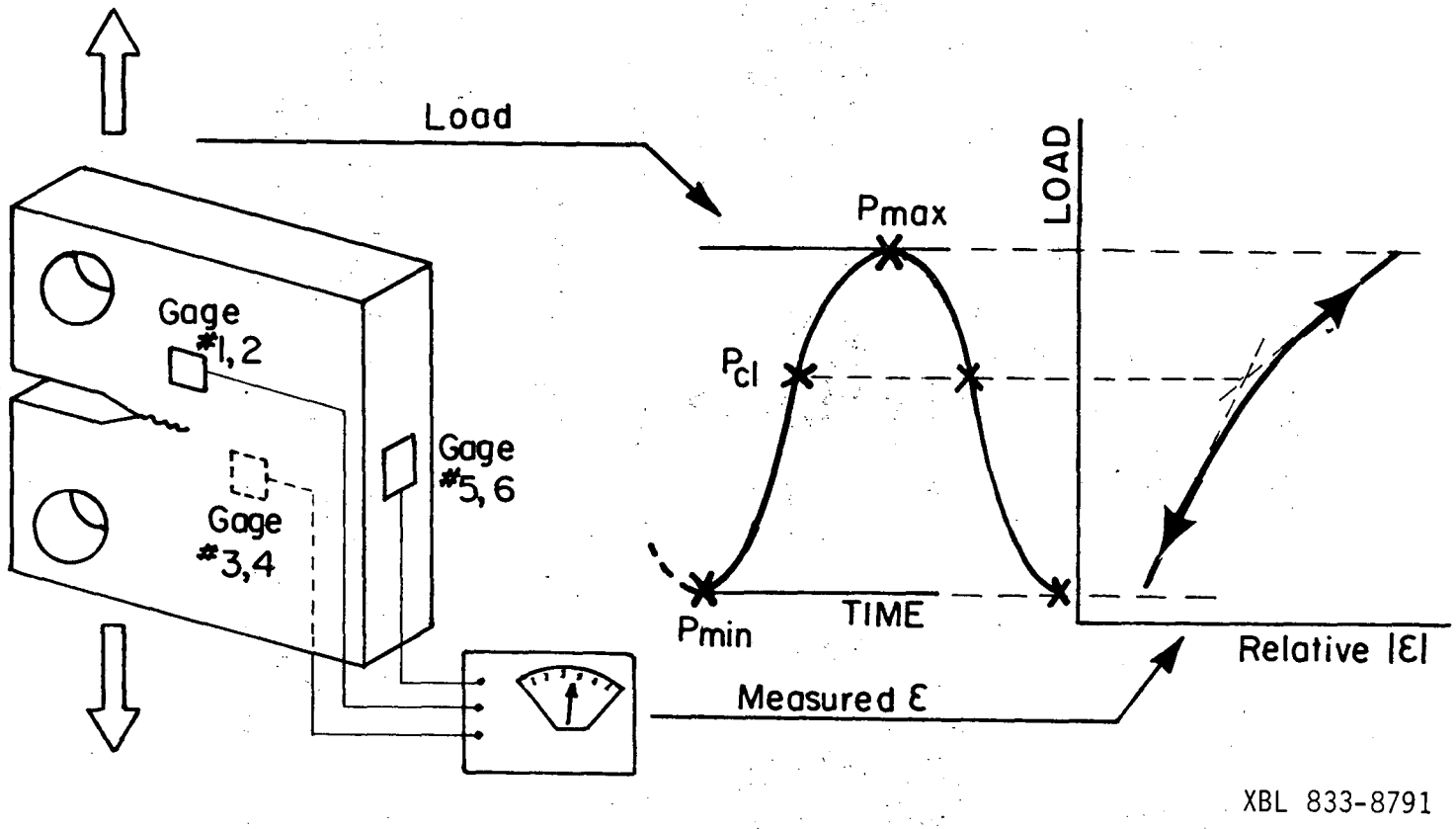

Fig. 2: Procedures for measuring crack closure showing a) the location of the strain gauges and b) elastic compliance curves of load versus relative strain $|\varepsilon|$ used to estimate the load at closure P_{cl}.

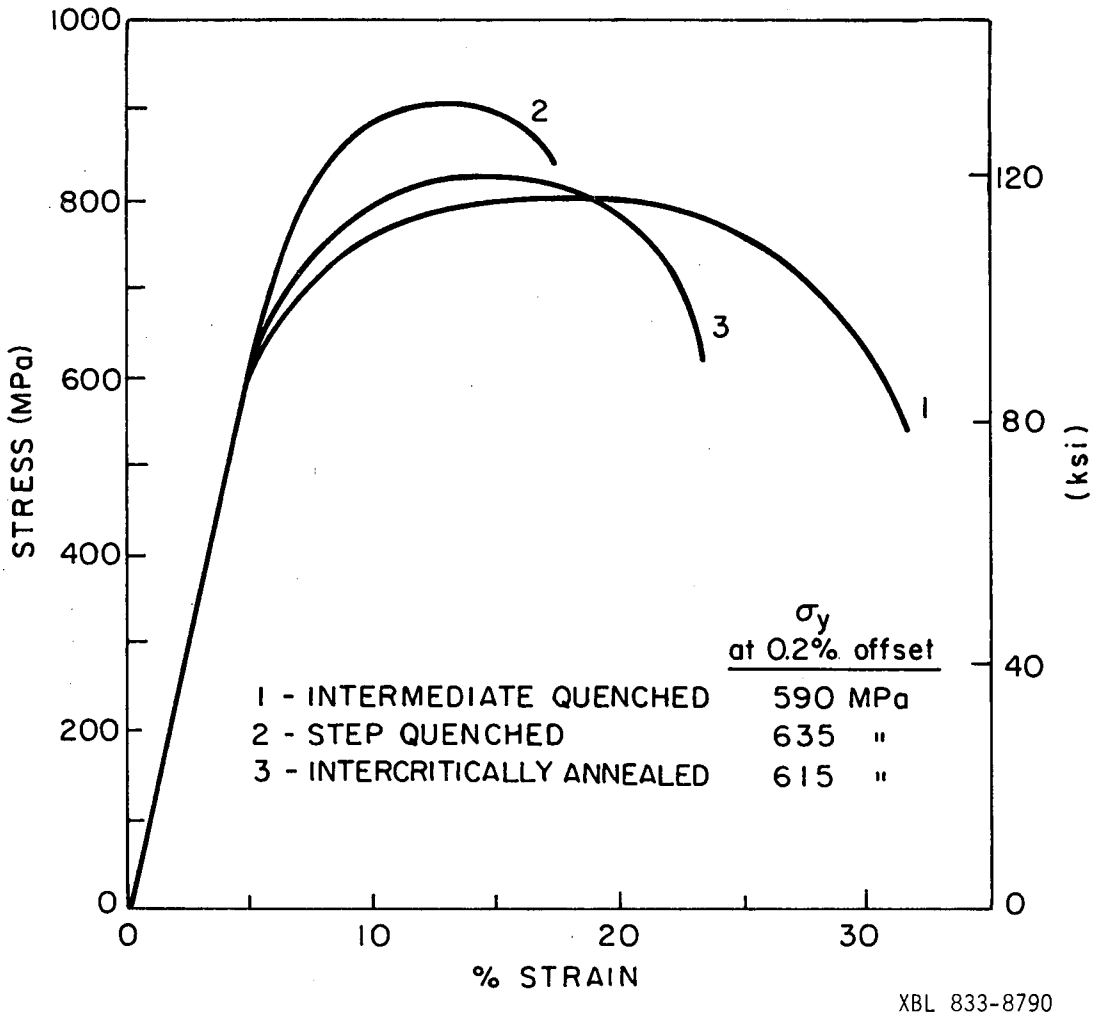

Fig. 3: Engineering stress-strain curves for uniaxial tensile tests in IQ, SQ and IA microstructures in Fe/2Si/0.1C dual-phase steel.

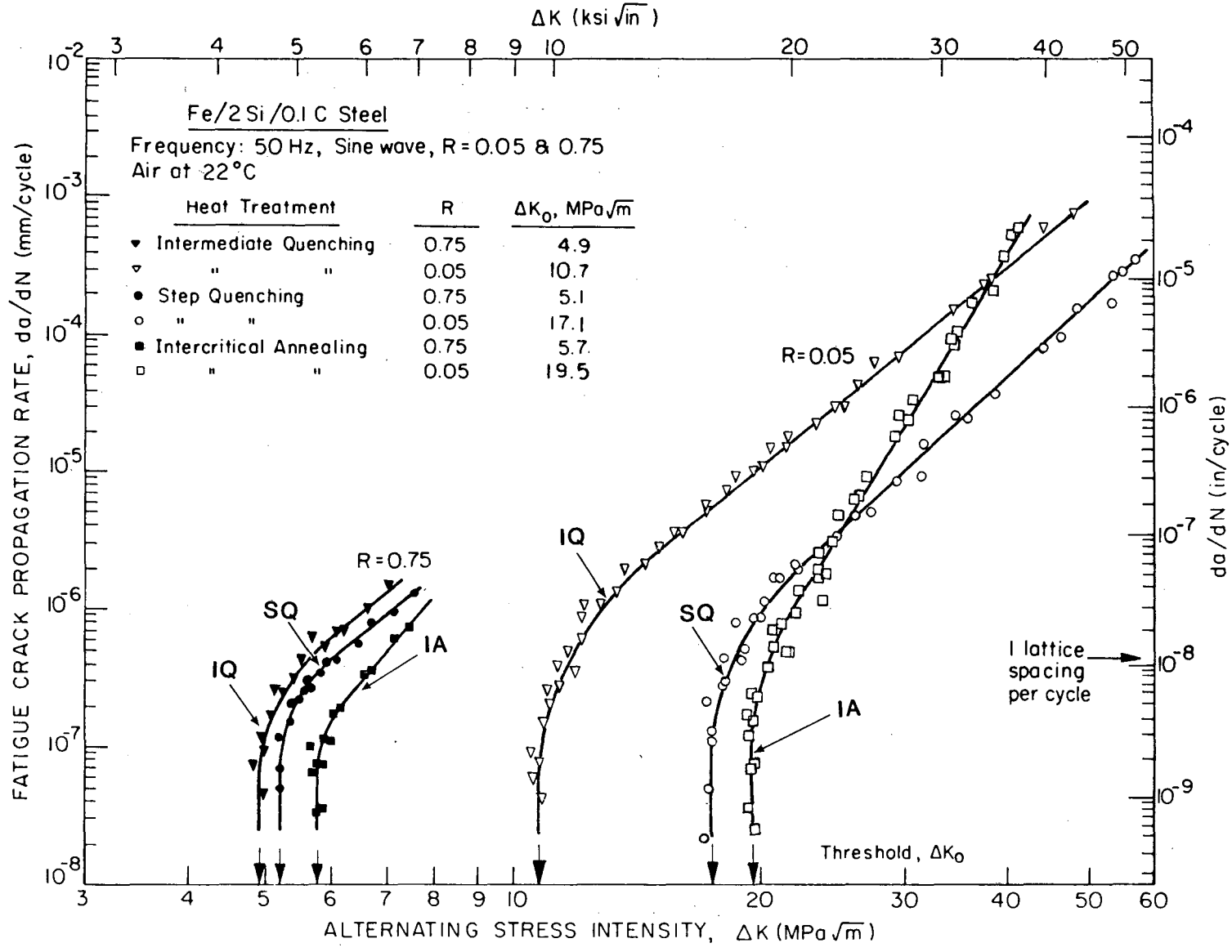

XBL 838-10897

Fig. 4: Variation in fatigue crack propagation rate (da/dN) with nominal stress intensity range (ΔK) for Fe/2Si/0.1C dual-phase steel with IQ, SQ and IA microstructures at load ratios of R = 0.05 and 0.75. Tests in room temperature moist air at 50 Hz frequency.

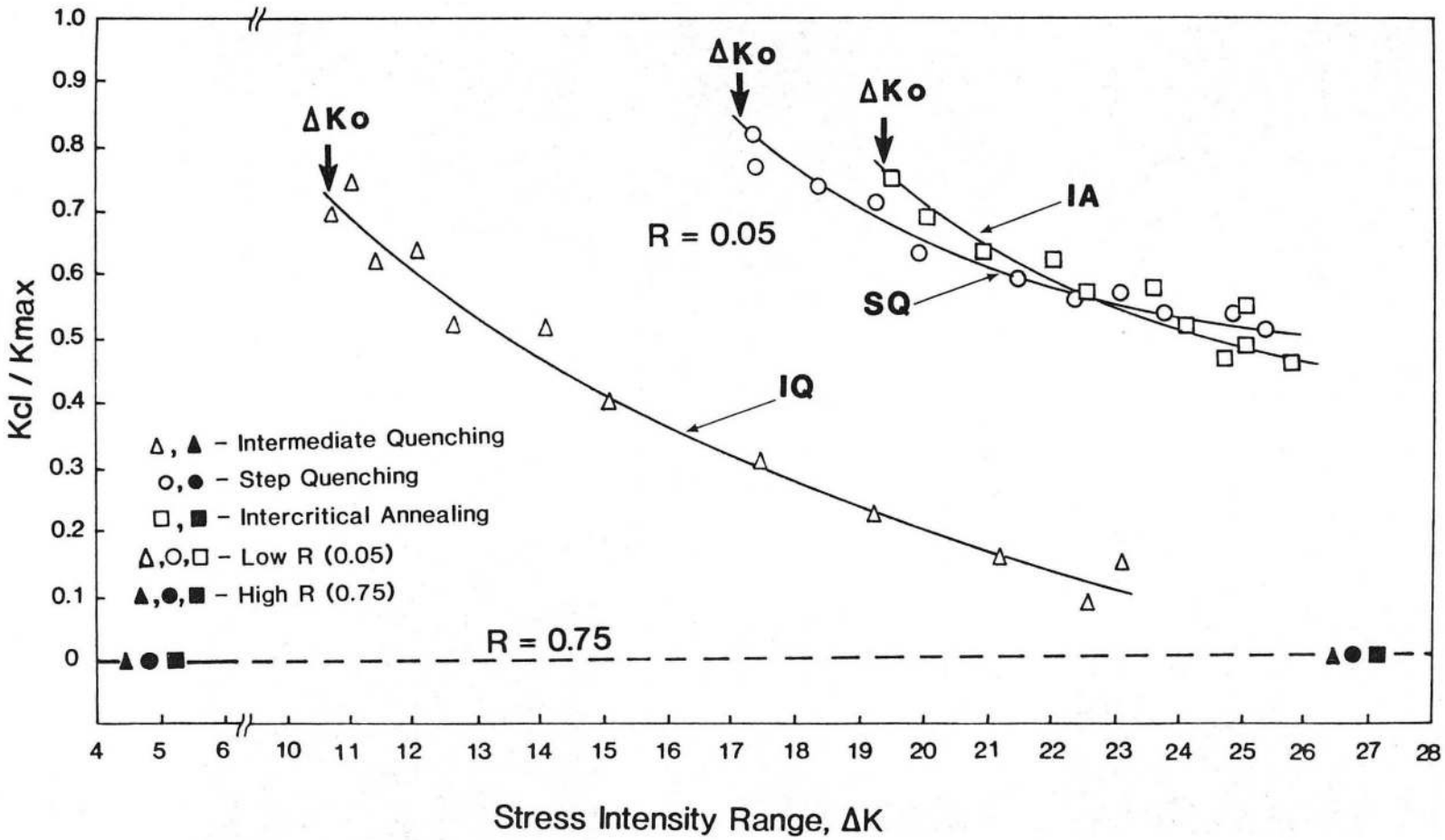

XBL 838-10896

Fig. 5: Experimental measurement of crack closure at R = 0.05 and 0.75 using elastic compliance curves from back-face and side-face strain gauges (Fig. 2) for IQ, SQ and IA microstructures. The degree of closure is expressed as the ratio of the closure to maximum stress intensity (K_{cl}/K_{max}) as a function of the nominal stress intensity range ΔK.

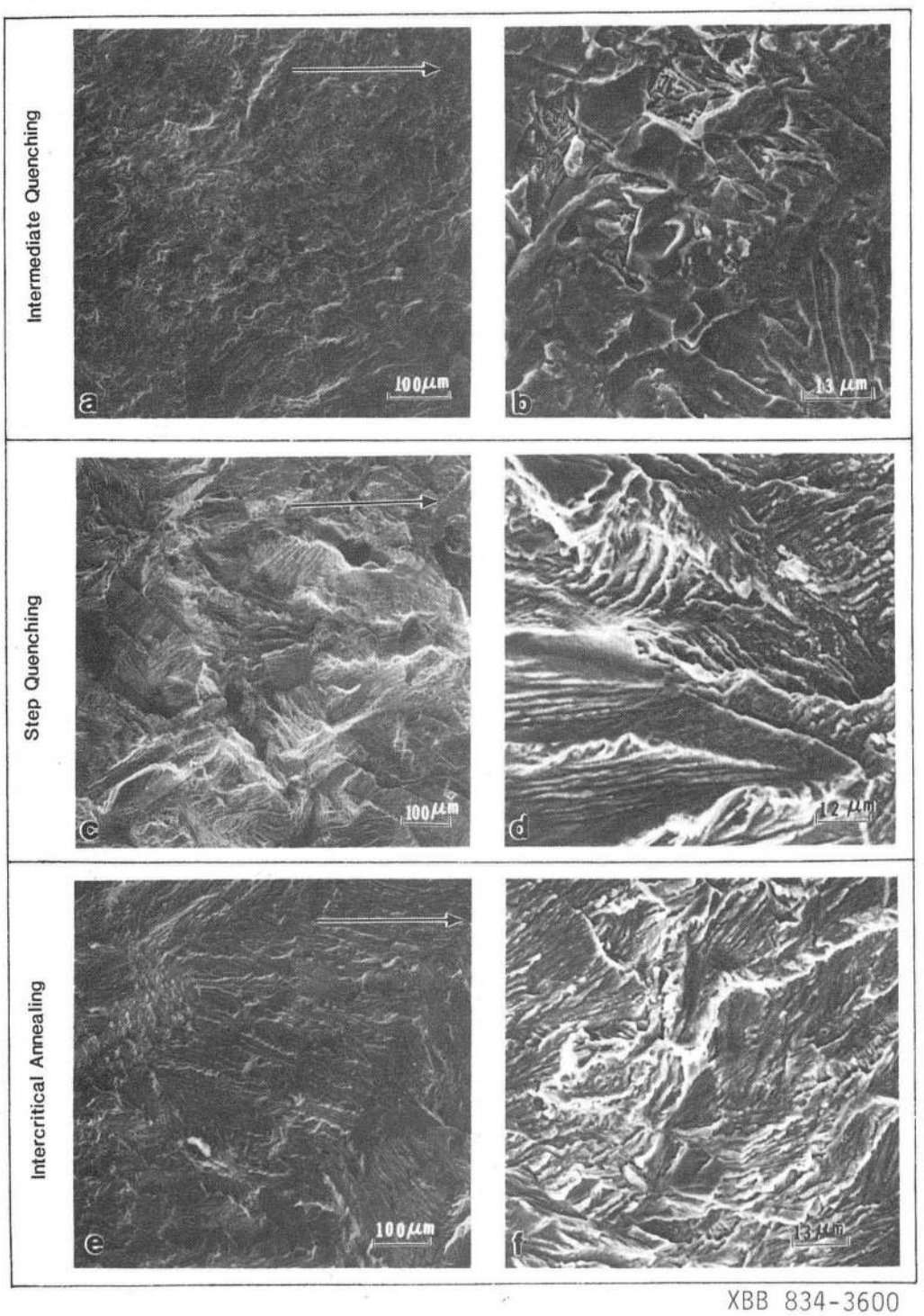

Fig. 6: Scanning electron micrographs of fatigue fracture surfaces close to the threshold ΔK_0 at R = 0.05 for (a)-(b) intermediate quenched (IQ), (c)-(d) step quenched (SQ) and (e)-(f) intercritical annealed (IA) microstructures. Note faceted appearance of fracture surfaces for SQ and IA microstructures. Arrow indicates general direction of crack growth.

Mid Growth Region :

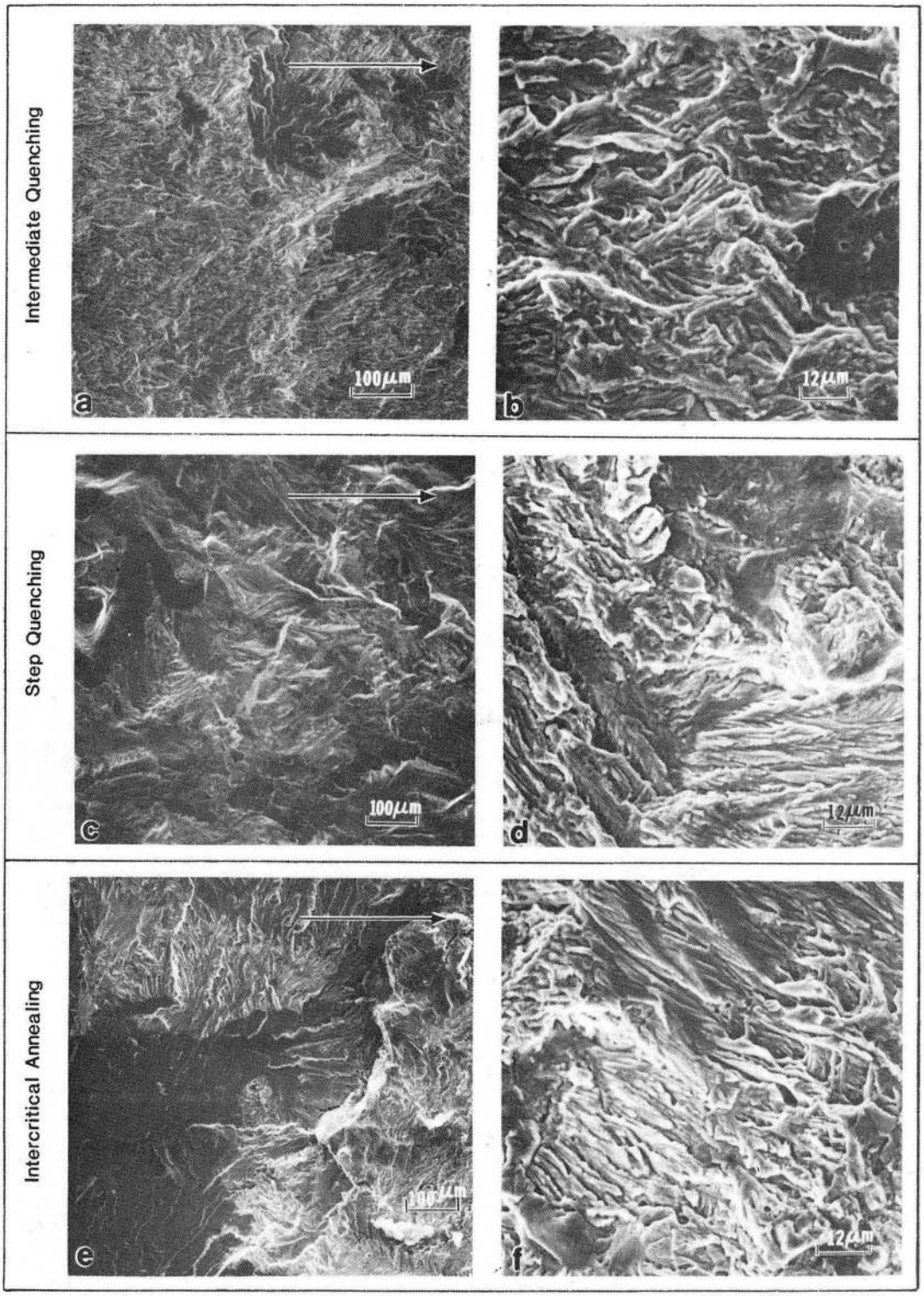

XBB 834-3599A

Fig. 7: Scanning electron micrographs of fatigue fracture surfaces at approximately da/dN $\sim$ 5 x 10^{-5} mm/cycle at R = 0.05 for (a)-(b) intermediate quenched (IQ), (c)-(d) step quenched (SQ) and (e)-(f) intercritical annealed (IA) microstructures. Note occurrence of transgranular cleavage facets for the IA microstructure. Arrow indicates general direction of crack growth.

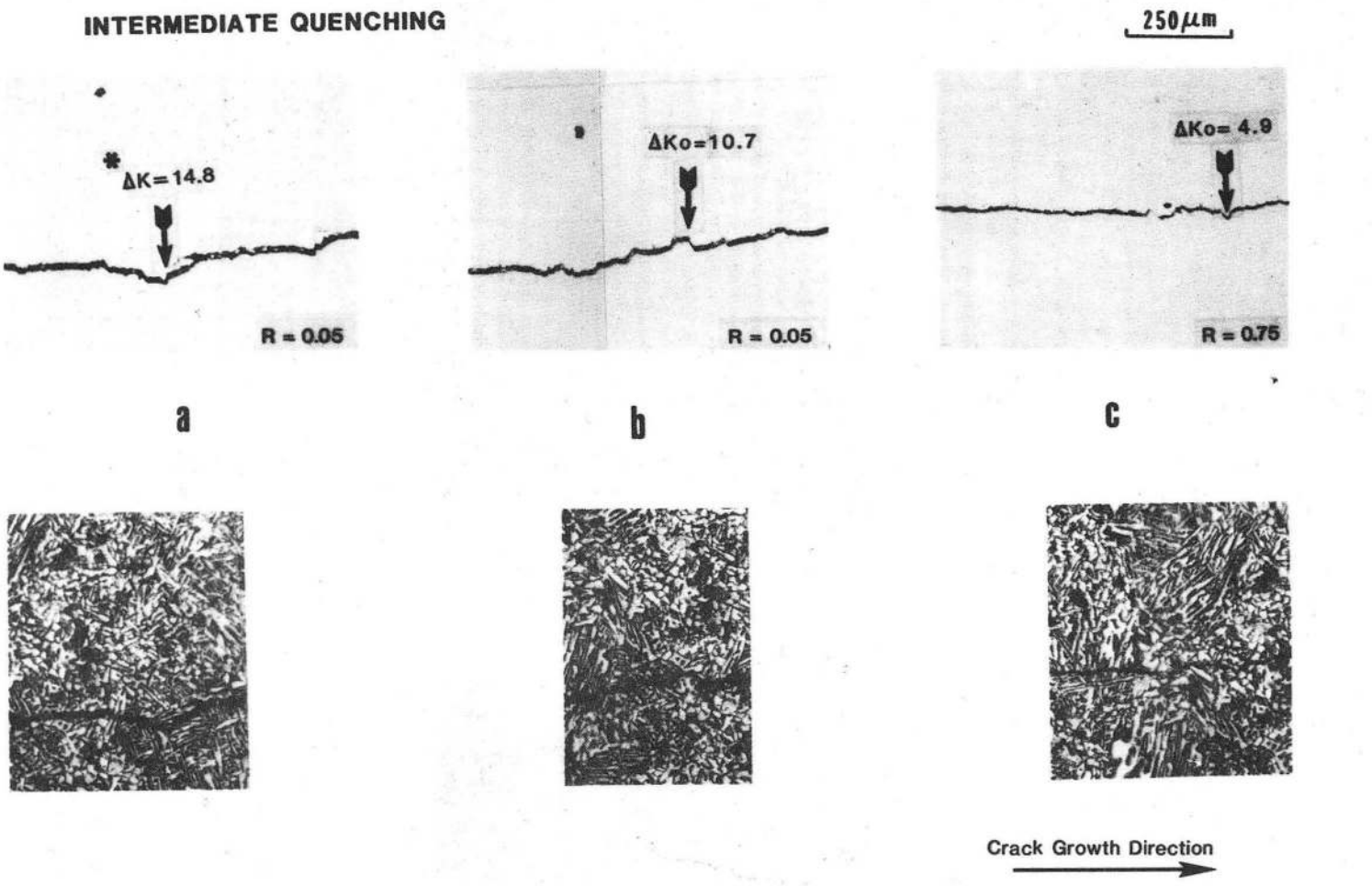

Fig. 8: Unetched and nital etched sections through the crack path in the intermediate quenched (IQ) structure a) at $\Delta K = 14.8$ MPa$\sqrt{m}$ ($R = 0.05$), b) at threshold at $R = 0.05$, and c) at threshold at $R = 0.75$.

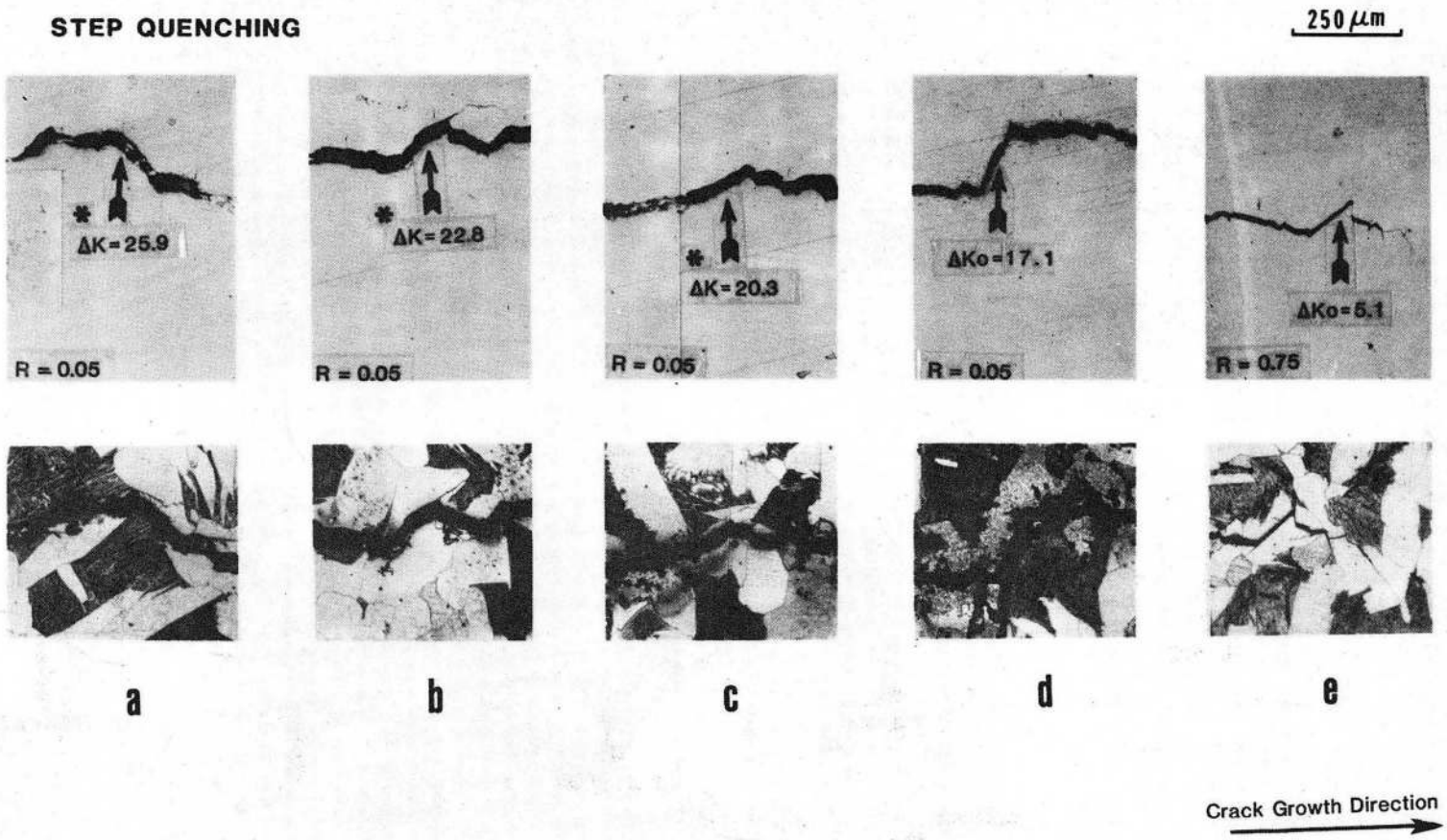

Fig. 9: Unetched and nital etched sections through the crack path in step quenched (SQ) structure, showing locations of marked crack deflections at a) ΔK = 25.9 MPa$\sqrt{m}$, b) ΔK = 22.8 MPa$\sqrt{m}$, and c) ΔK = 20.3 MPa$\sqrt{m}$, and final arrest at the threshold at d) R = 0.05 and e) R = 0.75.

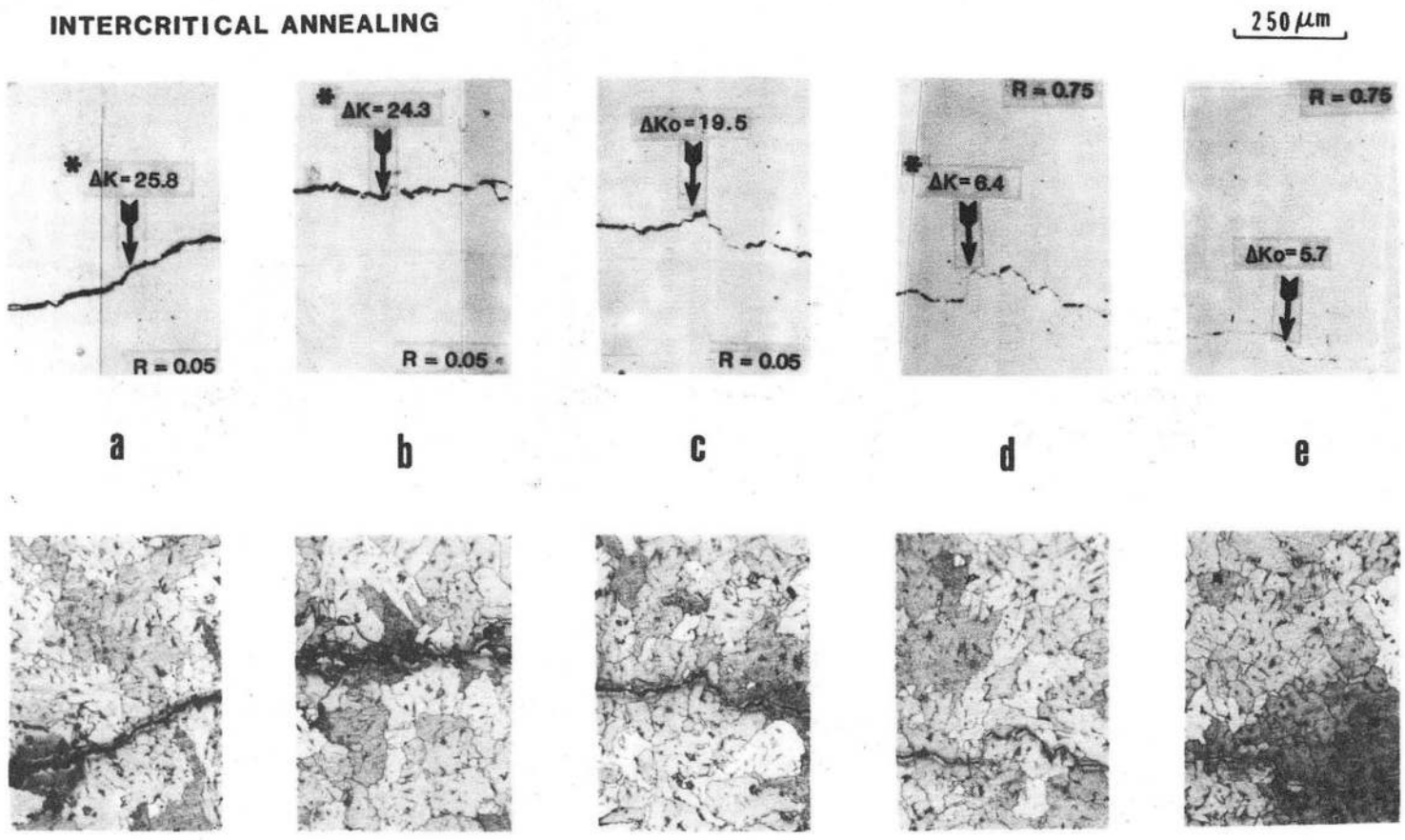

Fig. 10: Unetched and nital etched sections through the crack path in intercritical annealed (IA) structure, showing behavior at R = 0.05 at a) ΔK = 25.8 MPa$\sqrt{m}$, b) ΔK = 24.3 MPa$\sqrt{m}$, and c) final arrest at the threshold at ΔK_o = 19.5 MPa$\sqrt{m}$. d) and e) show the tortuous crack paths at 6.4 and 5.7 MPa$\sqrt{m}$, respectively at R = 0.75. Note significant deflections in the crack path.

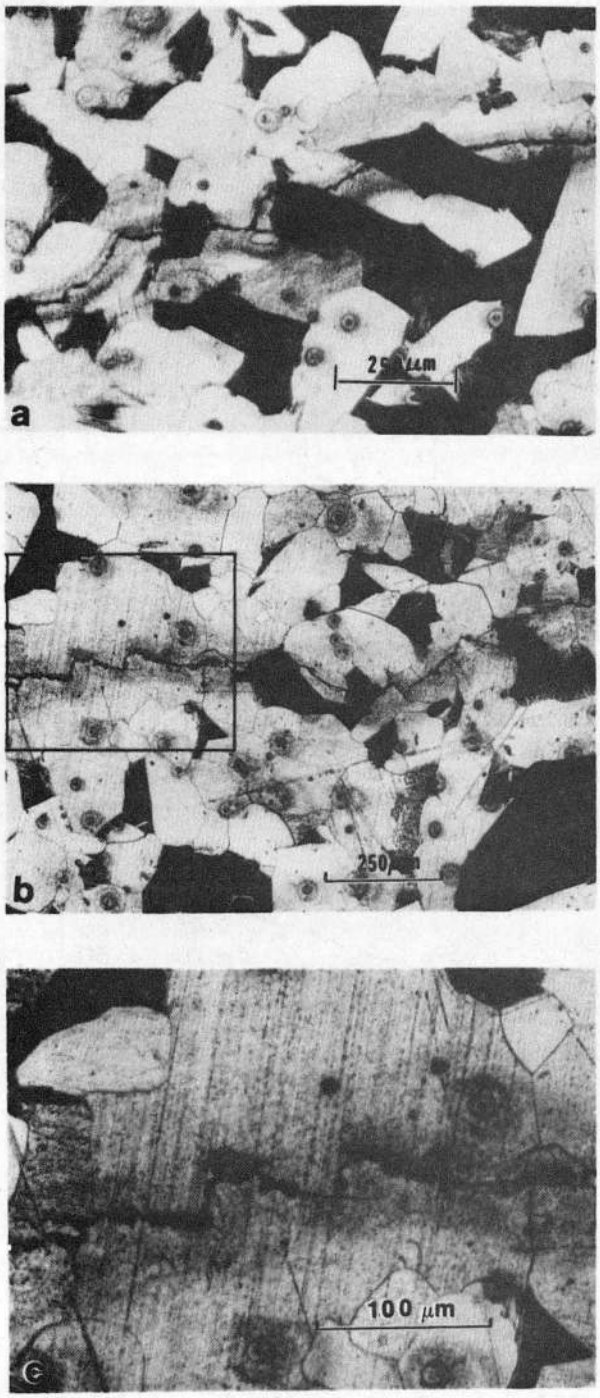

XBB 834-3303

Fig. 11: Example of significant crack path meandering and deflection in the step quenched (SQ) microstructure at near-threshold levels. The severe zig-zag or faceted appearance of the crack path, most clearly seen in c), occurs due to deflection at the ferrite grain boundaries.

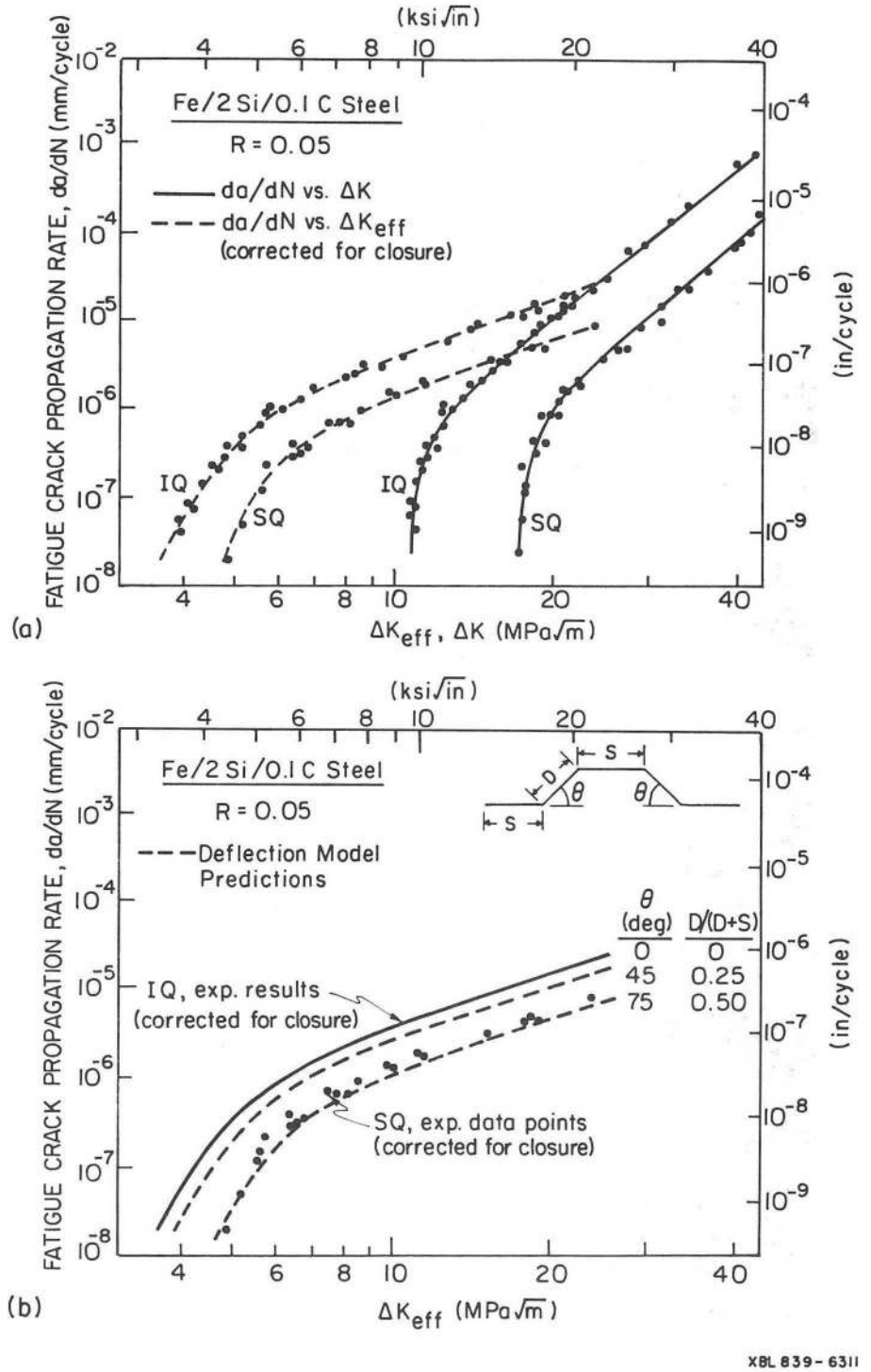

Fig. 12: Respective roles of crack closure and crack deflection on fatigue crack propagation behavior in dual phase Fe/2Si/0.1C steel at R = 0.05, showing a) experimental da/dN vs. ΔK data for IQ and SQ microstructures (from Fig. 4) corrected for closure to da/dN vs. ΔK_{eff} data using experimental closure measurements (Fig. 5) and b) predictions of the effect of crack deflection using two-dimensional linear elastic deflection model (ref. 30) with IQ data as reference with $\theta = 0°$ and $D/(D+S) = 0$, and taking $\theta \approx 45°$ to $75°$ with $D/(D+S) \approx 0.25$ to 0.50 for the SQ condition.

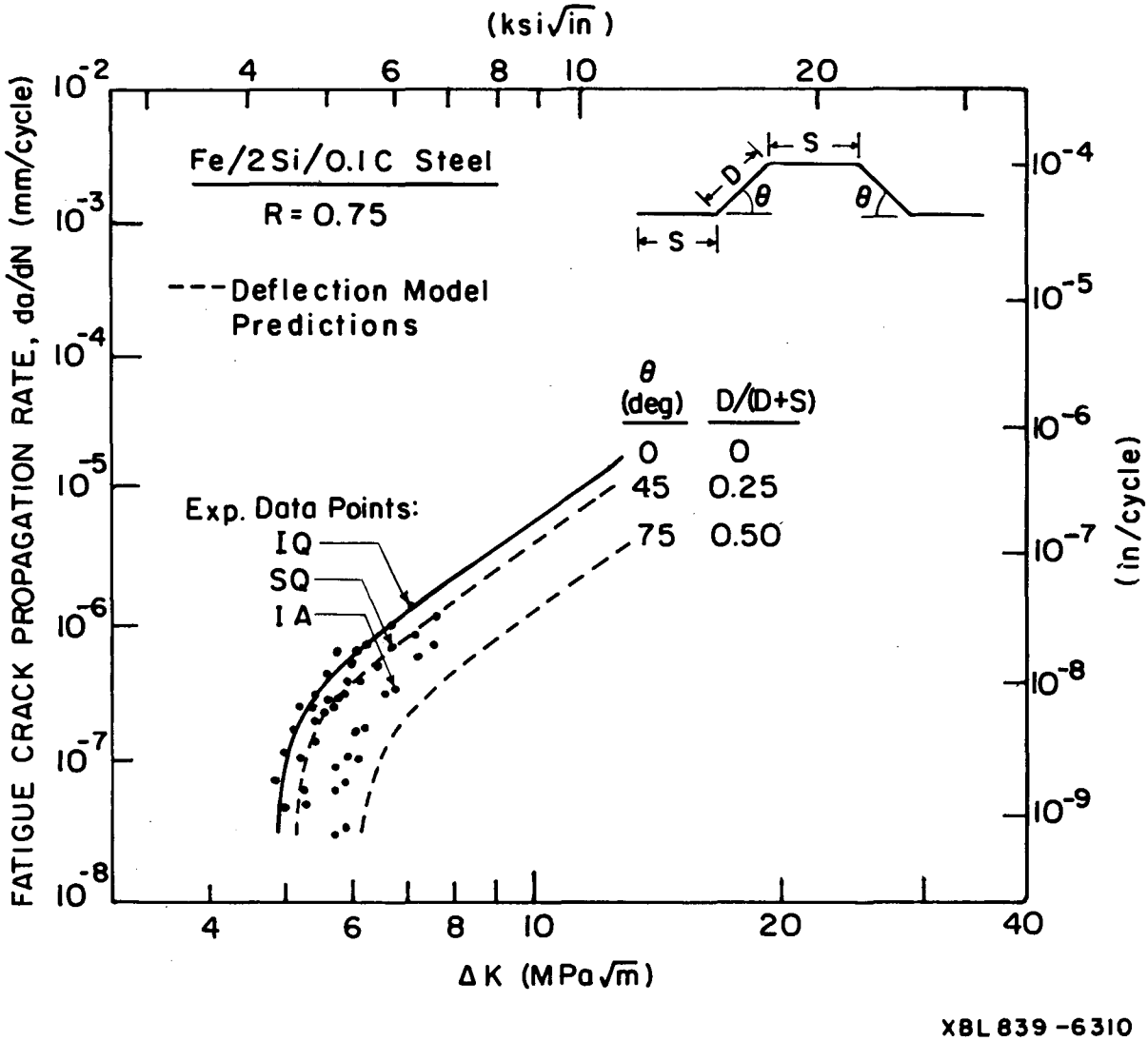

Fig. 13: Predicted role of crack deflection on fatigue crack propagation behavior in dual phase Fe/2Si/0.1C steel at R = 0.75, showing experimental data points for IQ, SQ and IA microstructures (from Fig. 4) and predictions of the effect of crack deflection using two-dimensional linear elastic deflection model (ref. 30). IQ data are taken as reference with $\theta = 0°$ and $D/(D+S) = 0$, and predictions are shown for $\theta \approx 45°$ to $75°$ with $D/(D+S) \approx 0.25$ to 0.50, representative of the SQ and IA conditions.

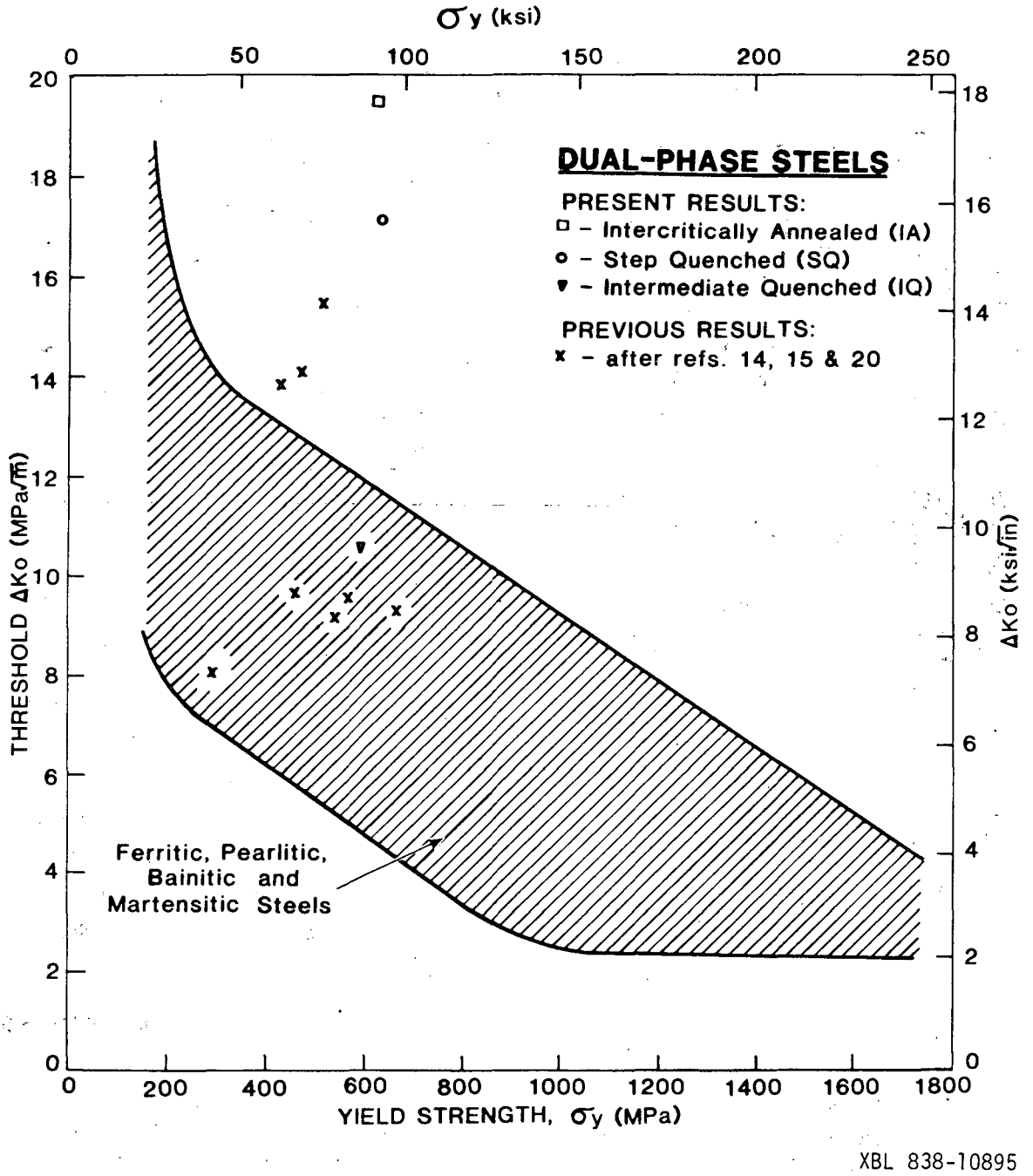

Fig. 14: Variation of fatigue threshold stress intensity range ΔK_0 at low load ratios ($R \sim 0$) as a function of monotonic yield strength σ_y for ferrous alloys. Scatter band shows long crack threshold data for ferritic, pearlitic, bainitic and martensitic steels, taken from tabulations in refs. 1 and 5. Data points show long crack threshold results for duplex ferritic/martensitic microstructures, indicating the exceptional strength and fatigue threshold properties of the present SQ and IA dual-phase structures.

TECHNICAL INFORMATION DEPARTMENT
LAWRENCE BERKELEY LABORATORY
UNIVERSITY OF CALIFORNIA
BERKELEY, CALIFORNIA 94720